Structural Changes of Hydroxylapatite during Plasma Spraying

Subjects: Chemistry, Medicinal

Contributor: Robert Heimann

Functional osseoconductive coatings based on hydroxylapatite (HAp) and applied preferentially by atmospheric plasma spraying to medical implant surfaces are a mainstay of modern implantology. During contact with the hot plasma jet, HAp particles melt incongruently and undergo complex dehydration and decomposition reactions that alter their phase composition and crystallographic symmetry, and thus, the physical and biological properties of the coatings. Surface analytical methods such as laser-Raman and nuclear magnetic resonance (NMR) spectroscopies are useful tools to assess the structural changes of HAp imposed by heat treatment during their flight along the hot plasma jet.

hydroxylapatite oxyhydroxylapatite oxyapatite tricalcium phosphate tetracalcium phosphate Raman spectroscopy MAS-CP NMR spectroscopy 2D-HETCOR NMR spectroscopy

1. Introduction

Among various bioactive calcium orthophosphates utilized in medical devices, hydroxylapatite (HAp) takes on particular important roles. Applications are ranging from coatings for hip and knee endoprostheses, to densified monolithic implants for dental root replacement, to bone cavity filler, to three-dimensional bone repair scaffolds, and to advanced hybrid hydroxylapatite-polymer nanocomposites with enhanced osseoconductive, angiogenic, and antimicrobial functions able to mimic salient biological properties. All this is based on the chemical and structural similarity of hydroxylapatite to the inorganic constituent of bone and teeth. Although non-stoichiometric biological apatite differs from stoichiometric geological apatite in terms of crystalline order, crystallite size, defect density, amount of hydroxyl anions, as well as degree of cationic and anionic substitution, synthesized hydroxylapatite serves well as a proxy for its natural counterpart. Osseoconductive hydroxylapatite coatings are being predominantly deposited on implant materials by atmospheric plasma spraying despite the fact that its crystallographic structure and phase composition suffers from exposure to the high temperature plasma jet. Hence, to achieve optimum biomedical performance of plasma-sprayed hydroxylapatite coatings in contact with living tissue, their structural alteration in the hot plasma jet must be carefully assessed and considered when designing coating systems for medical application.

Since hydroxylapatite coatings on medical implants will be in contact with extracellular fluid (ECF), their performance and structural changes were studied copiously in the past by Raman [1][2][3][4][5][6], nuclear magnetic resonance (NMR) [7][8][9][10][11], and X-ray photoelectron spectroscopies (XPS) [12]. Stammeier et al. [6] investigated the kinetics of the amorphous calcium phosphate (ACP) to crystalline HAp transformation at ambient temperature and pH = 9.2 by taking highly time-resolved in-situ Raman spectroscopy spectra at a rate of 100 spectra/h. Their results showed that after 18 h, transformation of ACP to crystalline HAp occurred as demonstrate in a peak shift from 950 to 960 cm^{-1} as well as in a sharpening of the 960 cm^{-1} peak. Likewise, solid-state NMR work by Jäger et al. [11] revealed that HAp nanoparticles possess a crystalline core with Ca/P = 1.67 akin to stoichiometric HAp but are covered by an approximately 1 nm thin disordered surface film with Ca/P~1.5 dominated by HPO_4^{2-} anions and structural water. This leads to the conclusion that the surface of n-HAp is critically different from bulk HAp, with important consequences for the ability to bind protein molecules essential for osseointegration. Solid-state NMR in conjunction with ab initio modelling has been found capable of fully describing the surface structure and chemistry of HAp, essential to understand its reactivity towards the organic matrix of bone [10].

2. Structure of Hydroxylapatite

Hydroxylapatite, $Ca_{10}(PO_4)_6(OH)_2$ is a member of a large group of chemically different but crystallographically identical compounds with the general formula $M_{10}(ZO_4)_6X_2$. Today, some sixty members with this structure are known as natural minerals as well as synthetic compounds. Large M cations are Ca, Sr, K, Na, Cd, Pb, Zn, La, Ce, and several others; small tetrahedrally coordinated Z cations entering the structure may be P, V, As, Cr, Si, C, Al, and S, whereas X are OH, Cl, F, CO_3, and H_2O, as well as vacancies □ that are located in the wide channels parallel to [00.1]. Hydroxylapatite crystallizes in the hexagonal space group $P6_3/m$ (S.G. 176). **Figure 1**A shows Ca_IO_9 polyhedra chains (grey) parallel to [00.1] with 6_3 screw characteristic. The chains share corners and edges with [PO_4] tetrahedra (green) to yield a hexagonal array. **Figure 1**B depicts details of the ion environment around the *c*-axis. Two oxygen ions of the [PO_4] tetrahedra are found above and below mirror planes through z = ¼ and z = ¾. The non-equivalent Ca^{2+} ions are located at two different positions: Ca_I at z = 0 and z = ½ along the three-fold axes a_i (Wyckoff position 4*f*), and Ca_{II} at z = ¼ and z = ¾ along the hexagonal screw axis 6_3 parallel [00.1] (Wyckoff position 6*h*). Hence, considering the two non-equivalent Ca positions, a more accurate formula of hydroxylapatite is $[(Ca_I)_4(Ca_{II})_6](PO_4)_6(OH)_2$. The X anions are located at z = ¼ and z = ¾. Their exact positions depend on their size: the smaller F^- anion in fluorapatite is positioned exactly at the center of the triangles formed by the three Ca_{II} cations, the larger OH^- anion in hydroxylapatite is off-center by an increment δ = 0.36 Å [13] (**Figure 1**B).

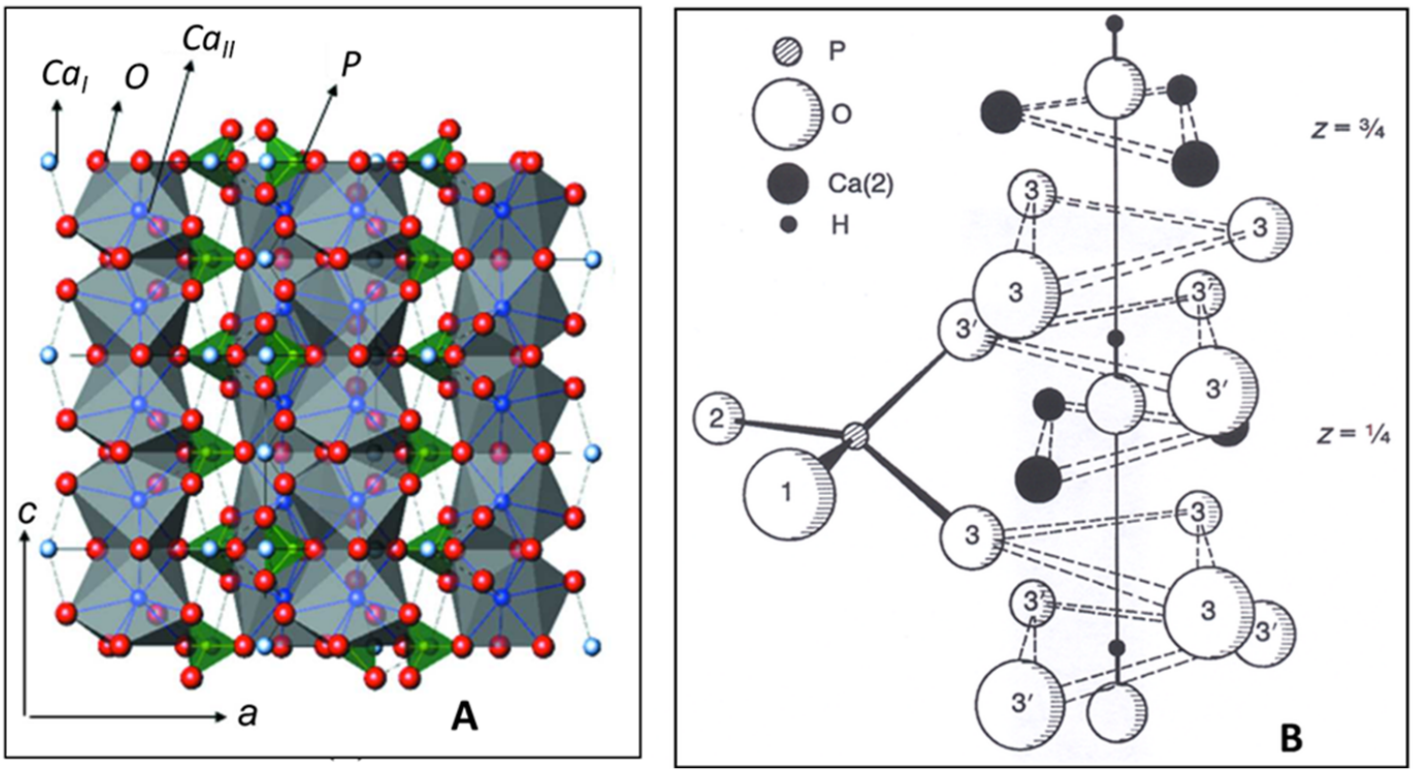

Figure 1. (**A**): Crystallographic structure of HAp with a hexagonal unit cell a = 0.9432 nm, c = 0.6881 nm [14]. Blue spheres: Ca^{2+}; green spheres: P^{5+}; red spheres: O^{2-}. Ca_IO_9 polyhedra chains parallel to [00.1] are linked by [PO_4] coordination tetrahedra. © Reproduced with permission of the International Union of Crystallography. (**B**): Details of the arrangement of the Ca_{II} ions at z = ¼ and ¾, and O^{2-} ions surrounding the 6_3 screw axis parallel to [00.1]. The OH^- anions are positioned within the triangular Ca_{II} configuration at z = ¼ + δ and z = ¾ + δ [15]. © Reprinted with permission from Elliott et al., Adv. X-ray Anal. 45, 172–181 (2002). Copyright 2002, JCPDS-International Centre for Diffraction Data.

3. Thermal Alteration during Plasma Spraying

Thermal exposure during their flight along the plasma jet renders HAp particles to melt incongruently, i.e., they do not melt uniformly by retaining their stoichiometric composition, but react and decompose to form two solids of different composition plus liquid. This is shown in the inset of the CaO-P_2O_5 phase diagram where at 1570 °C hydroxylapatite decomposes to form α-$Ca_3(PO_4)_2$, $Ca_4O(PO_4)_2$, and melt (**Figure 2**).

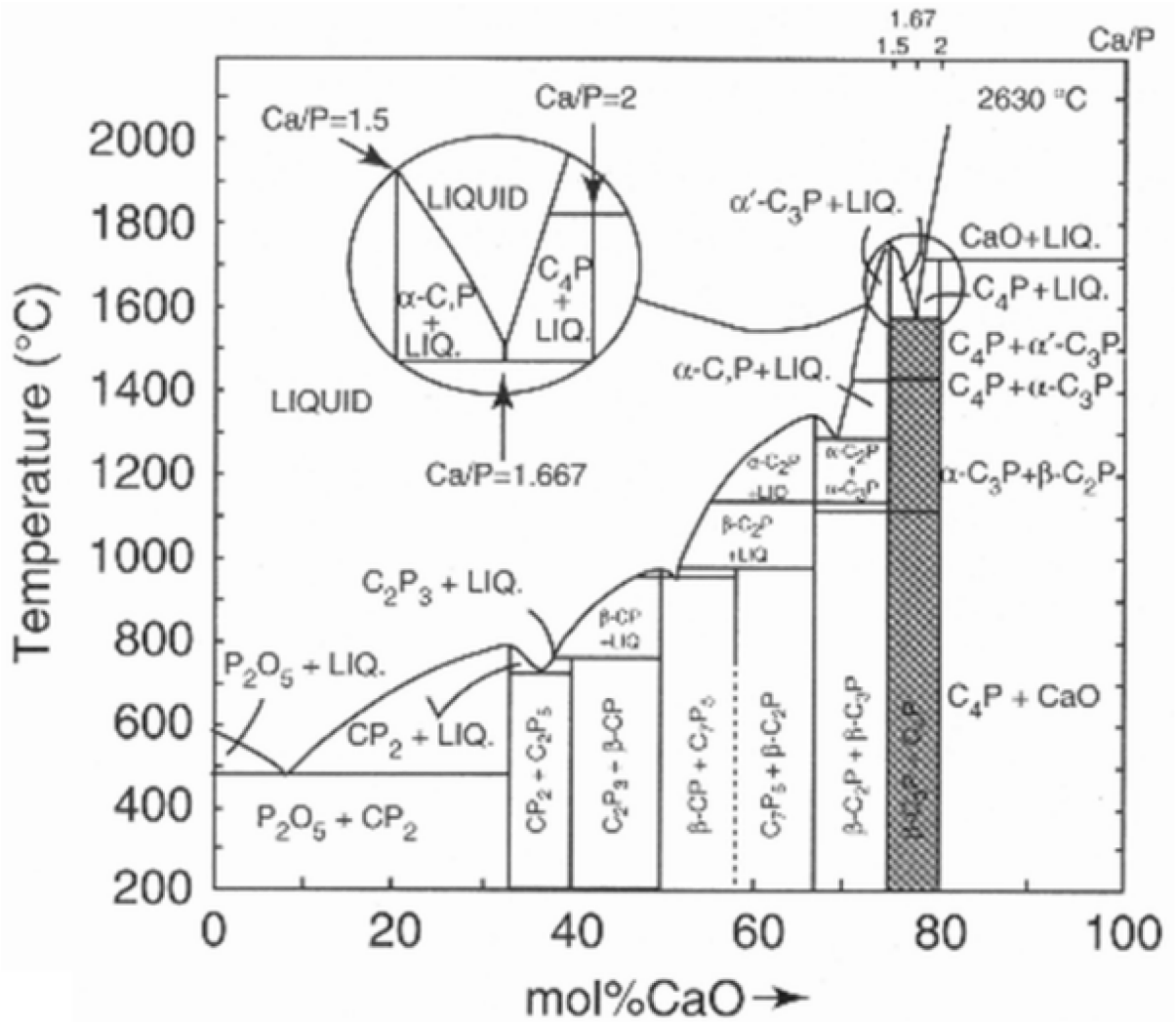

Figure 2. Phase diagram of the water-free binary system $CaO-P_2O_5$ showing the incongruent melting of hydroxylapatite with Ca/P = 1.667 (inset) [16]. The compositions are given in cement chemical notation, i.e., C = CaO, P = P_2O_5. © Reprinted with permission from E.R. Kreidler and F.A. Hummel, Inorg. Chem., 1967, 6(5), 884–891. Copyright 1967 Am. Chem. Soc.

Prolonged heating causes the calcium phosphate-containing liquid to lose volatile P_2O_5, thus shifting its composition along the liquidus line towards CaO-richer compositions. This process is accelerated by reduction reaction with hydrogen that is frequently added to the plasma-forming gases to increase the plasma enthalpy and, in turn, the heat transfer rate from the thermal plasma to the HAp powder particles flying along the center line of the plasma jet [17].

The stepwise thermal decomposition of HAp starts with a dehydration reaction that produces disordered oxyhydroxylapatite (OHAp) and eventually oxyapatite (OAp) according to Equations (1) and (2).

$$Ca_{10}(PO_4)_6(OH)_2 \rightarrow Ca_{10}(PO_4)_6(OH)_{2-2x}O_x\square_x + xH_2O, \quad (1)$$

$$Ca_{10}(PO_4)_6(OH)_{2-2x}O_x\square_x \rightarrow Ca_{10}(PO_4)_6O_x\square_x + (1-x)H_2O, \quad (2)$$

During thermal exposure, partially dehydrated hydroxylapatite (oxyhydroxylapatite, OHAp) was found to alter its crystallographic symmetry from the archetypical $P6_3/m$ to a triclinic $P\bar{1}$ space group when the amount of structurally bound hydroxyl groups is removed in excess of about 35% [18]. The reason for this triclinic distortion has been tentatively attributed to tilting of the hydroxyl ions located in the c-channels away from the channel axis. There are earlier statements that HAp retains its $P6_3/m$ space group up to a hydroxyl loss of 75%. Indeed, Liao et al. [19] reported that even a loss of chemically bound water as high as 75% retains the channel structure of apatite. The limiting composition is then $Ca_{10}(PO_4)_6(OH)_{0.5}O_{0.75}\square_{0.75}$ that corresponds to a water loss of 1.34% [20]. According to Alberius-Henning et al. [18], the degree of dehydration of 78% marks the onset of decomposition of the apatite structure. At this point, the unit cell parameters of OHAp with triclinic $P\bar{1}$ symmetry were determined to be a = 0.940023(3) nm, b = 0.939704(3) nm, c = 0.689967(72) nm, α = 90.0626(2)°, ß = 89.7478(1)°, and γ = 119.9971(2)°, very close to a hexagonal metric (**Table 1**). OHAp has been described formally either as a non-stoichiometric defect HAp [21][22] or a 1:1 solid solution of stoichiometric HAp and OAp [23].

Table 1. Crystallographic data of dehydration and decomposition products of hydroxylapatite. S.G. space group, HAp hydroxylapatite, m-HAp monoclinic hydroxylapatite, OHAp oxyhydroxylapatite, OAp oxyapatite, TTCP tetracalcium phosphate, TCP tricalcium phosphate. n.d. = not determined, * calculated crystallographical structures.

Phase	S.G.	a_0 (nm)	b_0 (nm)	c_0 (nm)	α (°)	ß (°)	γ (°)	Reference
HAp	P63/m	0.9432	0.9432	0.6881			120	[24]
HAp	P63/m	0.9418	0.9418	0.68827			120	[25]
c-empty *	P63/m	0.910	0.910	0.682			120.1	[26]
m-HAp	P21/b	0.9421	$2a_0$	0.6881			120	[27]
OHAp	$P\bar{1}$	0.9400	0.9397	0.6899	90.063	89.748	119.997	[18]
OAp	$P\bar{6}$	0.9432	0.9432	0.6881			120	[28]
OAp	$P\bar{6}$	n.d.	n.d.	0.6902			n.d.	[29]
OAp	$P\bar{6}$	n.d.	n.d.	0.6931			n.d.	[27]
OAp *	$P\bar{6}$	0.906	0.906	0.673	90.03	90.00	119.9	[26]
TTCP	P21	0.7023	1.1986	0.9473		90.901		[30]
α-TCP	P21/a	1.2873	2.7280	1.5213		126.208		[31]
ß-TCP	R3c	1.0435	1.0435	3.7403			120	[32]

[33]

complete [34], and neralogist Austin F. Rogers [35]. However, this elusive mineral was later correctly described as fluorapatite. Oxyapatite is known to convert back to HAp during cooling of the as-sprayed coating in the presence of moist air or by reacting with extracellular fluid (ECF) in vivo. This reaction is governed by the equation $O^{2-}(s) + \square(s) + H_2O(g) \rightarrow 2OH^-(s)$.

Although in the past the existence of oxyapatite as a thermodynamically stable compound has been questioned [36][37][38], some evidence to the contrary exists [20][39]. Trombe and Montel showed that OAp is only stable under vacuum or in water-free inert gases between 850 and 1050 °C, but decomposes beyond 1050 °C into tri- and tetracalcium phosphates [39]. Modelling using density-functional theory with local-density approximation (DFT-LDA) for considering the exchange and correlation parts of the electron interactions, and first-principles pseudopotentials for the electron-ion interactions has postulated a hexagonal defective 'c-empty' structure $Ca_{10}(PO_4)_6\square_2$ with a stable total energy minimum and an c_0 value of 0.682 nm [26]. Earlier studies have assumed in the structure of OAp a linear chain of O^{2-} ions parallel to [00.1], each one followed by a vacancy, conforming to a reduced space group of $\boldsymbol{P}6^{-}$ by loss of the mirror plane *m* as shown in **Figure 3**B [28].

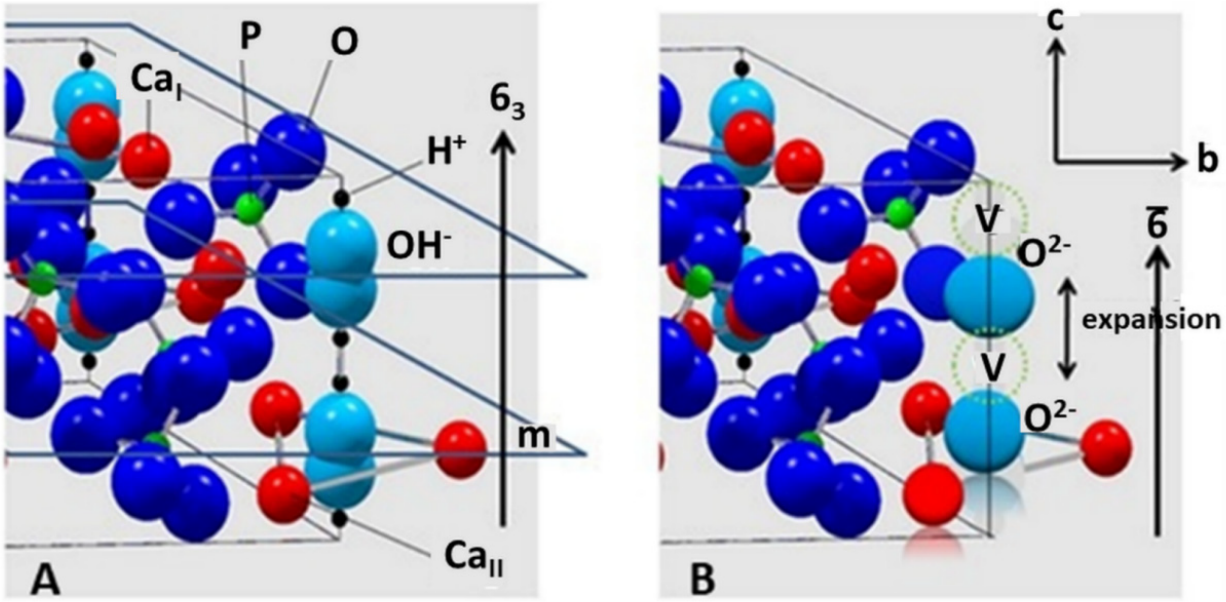

Figure 3. (**A**): Ball-and-spoke model of hydroxylapatite with space group $P6_3/m$. There are mirror planes *m* through $z = ¼$ and $z = ¾$, perpendicular to the *c*-axis with 6_3 characteristics. The non-equivalent Ca_I and Ca_{II} positions are indicated. (**B**): Hypothetical structure of oxyapatite, S.G. $\boldsymbol{P}6^{-}$. There is a chain of O^{2-} ions separated by vacancies V along the polar hexagonal axis 6^{-}. © Reprinted with permission from R.B. Heimann, Materialwiss. Werkstofftechn., 2009, 40(1–2), 23–30. Copyright 2009 Wiley.

Although the space group $\boldsymbol{P}6^{-}$ suggested by Alberius-Henning et al. [28] could be confirmed by the calculations of Calderin et al. [26], the c_0 value found by the former authors was only 0.673 nm, substantially shorter than that calculated by Calderin et al. and even shorter than the experimental value of 0.6930(8) nm obtained by Gross et al. [40] using synchrotron radiation (**Table 1**). Moreover, it was suggested by De Leeuw et al. that the formation of water or oxygen defects and a pile-up of oxygen vacancies in the c-channels (**Figure 3**B) is thermodynamically unfavorable [37]. In conclusion, the jury is still out whether oxyapatite could be considered a thermodynamically stable compound in the $CaO\text{-}P_2O_5$ phase diagram.

Unequivocal detection of OAp by conventional X-ray diffraction is difficult [41][42] since its *c*-axis dimension is only marginally larger than that of HAp [42][43][44]. This results in only a small shift of the (00.2) interplanar spacing

towards smaller diffraction angles. Consequently, very accurate measurements are needed as provided by single crystal diffraction using high-resolution synchrotron radiation or neutron diffraction. The lattice expansion during dehydration shown in **Figure 3**B is likely effected by the larger Shannon crystal radius of the O^{2-} ion (135 pm) compared to that of the OH^{-} ion (118 pm).

Additional investigation by the present author using synchrotron radiation [29] showed that atmospheric plasma spraying of stoichiometric HAp with comparatively low plasma power (11 kW) results in reversible dehydration, yielding OAp with c_0 = 0.6902(3) nm, somewhat longer compared to the value of c = 0. 6881 nm found for stoichiometric HAp. **Figure 4**A shows the synchrotron radiation diffraction pattern of plasma-sprayed HAp powder with mean grain size around 120 µm. The only crystalline phases detectable are OAp (Powder Diffraction File 04-011-1880 and 89-649) and ß-TCP (Powder Diffraction File 9-016978). However, the strongly elevated background between about 25 and 35 $^{o}2\theta$ with a centroid of 31 $^{o}2\theta$ suggests the presence of sizeable amounts of amorphous calcium phosphate (ACP). Quantitative estimation of the ACP content by the Keller and Dollase method [45] revealed ACP contributions of 25% (low plasma power: 11 kW) and 40% (high plasma power: 24 kW), respectively. **Figure 4**B shows the synchrotron diffraction pattern of the (00.2) and (00.4) interplanar spacings of HAp and OAp. Values of the scattering vectors Q of the (00.2) and (00.4) interplanar spacings obtained from the Powder Diffraction File are given for comparison, showing that the Q vectors measured are between those of HAp (PDF 9-432) and OAp (PDF 89-649). From the measured Q-values of 1.821 $Å^{-1}$ and 3.640 $Å^{-1}$, the c_0-values of OAp were calculated to be 0.6900(0) nm and 0.6904(6) nm, respectively, approximately 0.3% longer than that of HAp with 0.6881(4) nm. This confirms earlier data by Montel et al. [44].

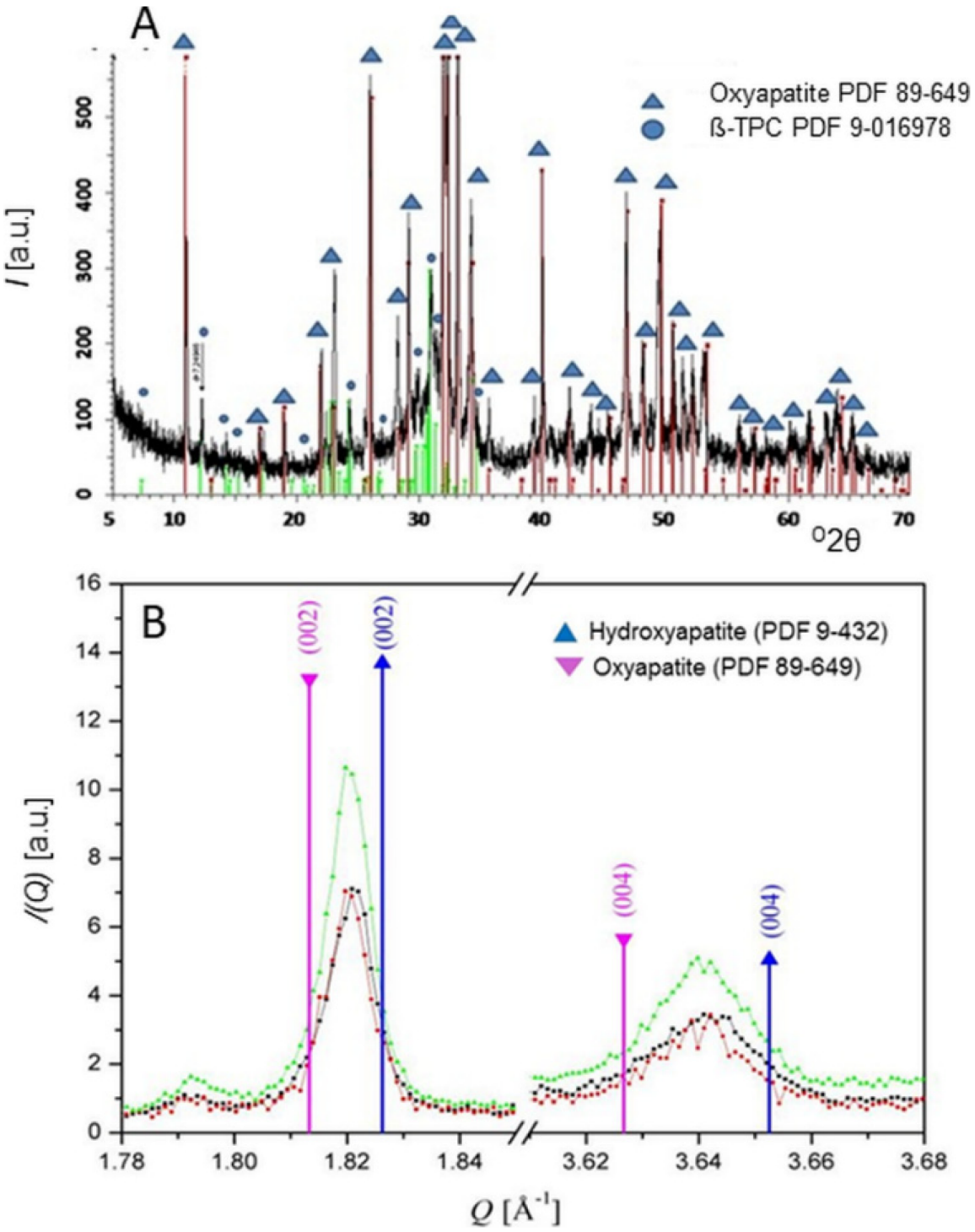

Figure 4. (**A**): High-resolution synchrotron radiation diffraction pattern of HAp coatings, deposited with low plasma power of 11 kW, show mainly oxyapatite with minor contribution of ß-tricalcium phosphate [29]. Additional plasma spray parameters were selected as follows: plasma gas (argon) flow rate 50 slpm, powder feed rate 18 g/min, spray distance 100 mm, and translation speed 30 m/min. (**B**): Scattering vectors Q (= $4\pi \times \sin\theta/\lambda$) of the diffraction profiles of three plasma-sprayed HAp coatings around (00.2) and (00.4) interplanar spacings of HAp (blue) and OAp (pink). Synchrotron radiation obtained from Angströmquelle Karlsruhe GmbH (ANKA), λ = 0.95 Å; step size 0.05 °2θ; range 2.0–52 °2θ. © Reprinted with permission from R.B. Heimann, Materialwiss. Werkstofftechn., 2009, 40(1–2), 23–30. Copyright 2009 Wiley.

During continuing exposure to high temperatures, OAp decomposes further to tricalcium phosphate (α-TCP) and tetracalcium phosphate (TTCP) [39] according to

$$Ca_{10}(PO_4)_6O_x\square_x \rightarrow 2\ \alpha\text{-}Ca_3(PO_4)_2 + Ca_4O(PO_4)_2. \quad (3)$$

Tetracalcium phosphate is the least stable calcium orthophosphate and crystallizes in the monoclinic space group P21. In its structure, the Ca^{2+} and $[PO_4]^{3-}$ ions are positioned in four sheets that are perpendicular to the *b*-axis. Each sheet contains two Ca^{2+}-$[PO_4]^{3-}$ columns and one Ca^{2+}-Ca^{2+} column, yielding an structural arrangement similar to glaserite, $K_3Na(SO_4)_2$. Two neighboring sheets constitute a structure closely related to the HAp structure [30].

At high plasma enthalpies, both α-TCP and TTCP further decompose, forming cytotoxic CaO according to

$$Ca_3(PO_4)_2 \rightarrow 3CaO + P_2O_5, \quad (4)$$

or

$$Ca_4O(PO_4)_2 \rightarrow 4CaO + P_2O_5. \quad (5)$$

Table 1 summarizes the space groups and unit cell parameters of HAp and its dehydration and decomposition phases considered in this contribution.

References

1. Silva, C.C.; Sombra, S. Raman spectroscopy measurements of hydroxyapatite obtained by mechanical alloying. J. Phys. Chem. Sol. 2004, 65, 1031–1033.
2. Ulian, G.; Valdrè, G.; Como, M.; Ugliengo, P. The vibrational features of hydroxylapatite and type A carbonated apatite: A first principle contribution. Am. Mineral. 2013, 98, 752–759.
3. Nosenko, V.V.; Yaremko, A.M.; Dzhagan, V.M.; Vorona, I.P.; Romanyuk, Y.A.; Zatovsky, I.V. Nature of some features in Raman spectra of hydroxyapatite-containing materials. J. Raman Spectrosc. 2016, 47, 726–730.
4. Antonakos, A.; Liarokapis, E.; Kyriacou, A.; Leventouri, T. Raman and IR studies of the effect of Fe substitution in hydroxyapatite and deuterated hydroxyapatite. Am. Mineral. 2017, 102, 85–91.
5. Mohonta, S.K.; Maria, K.H.; Rahman, S.; Das, H.; Hoque, S.M. Synthesis of hydroxyapatite nanoparticles and role of its site in hydroxyapatite/chitosan-gelatin biocomposite for bone grafting. Int. Nano Lett. 2021.
6. Stammeier, J.A.; Purgstaller, B.; Hippler, D.; Mavromatis, V.; Dietzel, M. In-Situ Raman spectroscopy of amorphous calcium phosphate to crystalline hydroxyapatite transformation. MethodsX 2018, 5, 1241–1250.

7. Rothwell, W.P.; Waugh, J.S.; Yesinowski, J.P. High-resolution variable-temperature 31P NMR of solid calcium phosphates. J. Am. Chem. Soc. 1980, 102, 2637–2643.
8. Yesinowski, J.P.; Wolfgang, R.A.; Mobley, M.J. New NMR methods for the study of hydroxyapatite surfaces. In Adsorption on and Surface Chemistry of Hydroxyapatite; Misra, D.N., Ed.; Springer: Boston, MA, USA, 1984; pp. 151–175.
9. Mason, H.E.; Kozlowski, A.; Phillips, B.L. Solid-state NMR study of the role of H and Na in AB-type carbonate hydroxylapatite. Chem. Mater. 2007, 20, 294–302.
10. Chappell, H.; Duer, M.; Groom, N.; Pickard, C.; Bristowe, P. Probing the surface structure of hydroxyapatite using NMR spectroscopy and first principles calculations. Phys. Chem. Chem. Phys. 2008, 10, 600–606.
11. Jäger, C.; Welzel, T.; Meyer-Zaika, W.; Epple, M. A solid-state NMR investigation of the structure of nanocrystalline hydroxyapatite. Magn. Reson. Chem. 2006, 44, 573–580.
12. Lu, H.B.; Campbell, C.T.; Graham, D.J.; Ratner, B.D. Surface characterization of hydroxyapatite and related calcium phosphates by XPS and TOF-SIMS. Anal. Chem. 2000, 72, 2886–2894.
13. Young, R.A.; Elliott, J.C. Atomic-scale bases for several properties of apatites. Arch. Oral Biol. 1966, 11, 699–707.
14. Veselinovic, L.; Karanovic, L.; Stojanovic, Z.; Bracko, I.; Markovic SIgnatovic, N.; Uskokovic, D. Crystal structure of cobalt-substituted calcium hydroxyapatite nanopowders prepared by hydrothermal processing. J. Appl. Cryst. 2010, 43, 320–327.
15. Elliott, J.C.; Wilson, R.M.; Dowker, S.E.P. Apatite structures. Adv. X-ray Anal. 2002, 45, 172–181.
16. Kreidler, E.R.; Hummel, F.A. Phase relations in the system SrO-P2O5 and the influence of water vapor on the formation of Sr4P2O9. Inorg. Chem. 1967, 6, 884–891.
17. Heimann, R.B. Plasma Spray Coating. Principles and Applications, 2nd ed.; Wiley-VCH: Weinheim, Germany, 2008; p. 34.
18. Alberius-Henning, P.; Adolfson, E.; Grins, J.; Fitch, A. Triclinic oxy-hydroxyapatite. J. Mater. Sci. 2001, 36, 663–668.
19. Liao, C.J.; Lin, F.H.; Chen, K.S.; Sun, J.S. Thermal decomposition and reconstruction of hydroxyapatite in air atmosphere. Biomaterials 1999, 20, 1807–1813.
20. Trombe, J.C.; Montel, G. Sur la preparation de l’oxyapatite phosphocalcique. Comptes Rendus Séances l’Académie Sci. (Paris) Série C 1971, 273, 452–465.
21. Hartmann, P.; Jäger, C.; Barth, S.; Vogel, J.; Meyer, K. Solid state NMR, X-ray diffraction, and infrared characterization of local structure in heat-treated oxyhydroxylapatite microcrystals: An

analogy of the thermal deposition of hydroxyapatite during plasma-spray procedure. J. Solid State Chem. 2001, 160, 460–468.

22. Heimann, R.B.; Tran, H.V.; Hartmann, P. Laser-Raman and Nuclear Magnetic Resonance (NMR) studies on plasma-sprayed hydroxyapatite coatings: Influence of bioinert bond coats on phase composition and resorption kinetics in simulated body fluid. Entwickl. Fert. Prüfung Eig. Anwend. Tech. Werkst. 2003, 34, 1163–1169.
23. Kijima, T.; Tsutsumi, M. Preparation and thermal properties of dense polycrystalline oxyhydroxyapatite. J. Am. Ceram. Soc. 1979, 62, 455–460.
24. Posner, A.S.; Perloff, A.; Diorio, A.F. Refinement of the hydroxyapatite structure. Acta Cryst. 1958, 11, 308–309.
25. Tas, A.C. X-ray diffraction data for flux-grown calcium hydroxyapatite whiskers. Powder Diffr. 2001, 16, 102–106.
26. Calderin, L.; Stott, M.J.; Rubio, A. Electronic and crystallographic structure of apatite. Phys. Rev. B 2003, 67, 134106–134112.
27. Elliott, J.C.; Mackie, P.E.; Young, R.A. Monoclinic hydroxylapatite. Science 1973, 180, 1055–1057.
28. Alberius-Henning, P.; Landa-Canovas, A.; Larsson, A.K.; Lidin, S. The structure of oxyapatite solved by HREM. Acta Crystallogr. B 1999, 55, 170–176.
29. Heimann, R.B. Characterisation of as-sprayed and incubated hydroxyapatite coatings with high resolution techniques. Mater. Werkst. 2009, 40, 23–30.
30. Dickens, B.; Brown, W.E.; Kruger, G.J.; Stewart, J.M. Ca4(PO4)2O, tetracalcium diphosphate monoxide. Crystal structure and relationships to Ca5(PO4)3OH and K3Na(SO4)2. Acta Cryst. 1973, 29, 2046–2056.
31. Yashima, M.; Kawaike, Y.; Tanaka, M. Determination of precise unit cell parameters of the α-tricalcium phosphate Ca3(PO4)2 through high-resolution synchrotron powder diffraction. J. Am. Ceram. Soc. 2007, 90, 272–274.
32. Yashima, M.; Sakai, A.; Kamiyama, T.; Hoshikawa, A. Crystal structure analysis of ß-tricalcium phosphate Ca3(PO4)2 by neutron diffraction. J. Solid State Chem. 2003, 175, 272–277.
33. Hendricks, S.B.; Hill, W.A.; Jakobs, K.D.; Jefferson, M.E. Structural characteristics of apatite-like substances and composition of phosphate rock and bone as determined from microscopical and X-ray examinations. Ind. Eng. Chem. 1931, 23, 1413–1418.
34. Voelcker, J.A. Die chemische Zusammensetzung des Apatits nach eigenen vollständigen Analysen. Ber. Dtsch. Chem. Ges. 1883, 16, 2460–2464.

35. Rogers, A.F. A new locality for voelckerite and the validity of voelckerite as a mineral species. Mineral. Mag. J. Mineral. Soc. 1914, 17, 155–162.
36. Bredig, M.A.; Franck, H.H.; Füldner, H. Beiträge zur Kenntnis der Kalk-Phosphorsäure-Verbindungen II. Z. Für Elektrochem. Angew. Phys. Chem. 1933, 39, 959–969.
37. De Leeuw, N.; Bowe, J.R.; Rabone, J.A.L. A computational investigation of stoichiometric and calcium-deficient oxy- and hydroxyapatite. Faraday Disc. 2007, 134, 195–214.
38. McConnell, D.; Hey, M.H. The oxyapatite (voelckerite) problem. Min. Mag. 1969, 37, 301–303.
39. Trombe, J.C.; Montel, G. Some features of the incorporation of oxygen in different oxidation states in the apatite lattice. I. On the existence of calcium and strontium oxyapatite. J. Inorg. Nucl. Chem. 1978, 40, 15–21.
40. Gross, K.A.; Berndt, C.C.; Stephens, P.; Dinnebier, R. Oxyapatite in hydroxyapatite coatings. J. Mater. Sci. 1998, 33, 3985–3991.
41. Gross, K.A.; Ben-Nissan, B.; Walsh, W.R.; Swarts, E. Analysis of retrieved hydroxyapatite coated orthopaedic implants. In Thermal Spray. Meeting the Challenges of the 21st Century; Coddet, C., Ed.; ASM International: Almere, The Netherlands, 1998; pp. 1133–1138.
42. Gross, K.A.; Berndt, C.C. Thermal processing of hydroxyapatite for coating production. J. Biomed. Mater. Res. 1998, 39, 580–587.
43. Trombe, J.C. Contribution á l’étude de la decomposition et de la réactivité de certaines apatites hydroxylées et carbonates. Ann Chim. (Paris) 1973, 8, 335–347.
44. Montel, G.; Bonel, G.; Trombe, J.C.; Heughebaert, J.C.; Rey, C. Progress dans le domaine de la chimie des composes phosphores solides a structure d’apatite. Pure Appl. Chem. 1980, 52, 973–987.
45. Keller, L.; Dollase, W.A. X-ray determination of crystalline hydroxyapatite to amorphous calcium phosphate ratio in plasma sprayed coatings. J. Biomed. Mater. Res. 2000, 49, 244–249.